Article

Discovery Medicine 2024; 36(181): 402–414
https://doi.org/10.24976/Discov.Med.202436181.38

IGF-1 Regulates Skeletal Muscle Degradation and Remolding in Ventilator-Induced Diaphragmatic Dysfunction by Mediating *FOXO1* Expression

Luyu Yang[1,†], Xiaohong Jiang[2,†], Shouzhi Fu[1,*], Jinhui Tan[3,*], Wankang Dian[1], Yumei Zhou[4]

[1]Department of ICU/Emergency, Wuhan Third Hospital & Tongren Hospital of Wuhan University, 430070 Wuhan, Hubei, China
[2]Department of Surgery, China University of Geosciences (Wuhan) Hospital, 430070 Wuhan, Hubei, China
[3]Department of Anesthesia, Wuhan Third Hospital & Tongren Hospital of Wuhan University, 430070 Wuhan, Hubei, China
[4]Department of Emergency, Wuhan Third Hospital & Tongren Hospital of Wuhan University, 430070 Wuhan, Hubei, China
*Correspondence: 18674096628@163.com (Jinhui Tan); fszfsz181@163.com (Shouzhi Fu)
[†]These authors contributed equally.
Published: 20 February 2024

Background: Mechanical ventilation (MV) sustains life in critically ill patients by providing adequate alveolar ventilation. However, prolonged MV could induce inspiratory muscle atrophy known as ventilator-induced diaphragmatic dysfunction (VIDD). Insulin-like growth factor (*IGF*)-*1* has been proven to play crucial roles in regulating skeletal muscle size and function. Meanwhile, the forkhead box protein O1 (*FOXO1*) has been linked to muscle atrophy. This study aimed to explore the effect of *IGF-1* on muscle degradation and remodeling in VIDD and delved into the association of the underlying mechanism involving *FOXO1*. Methods: VIDD models were established by treating rats with MV. Adeno-associated virus (AAV) was used for transfection to construct *IGF-1* and/or *FOXO1* overexpressed rats. There were four groups in this study: normal rats (NC), normal rats with MV treatment (MV), *IGF-1*-overexpressed rats with MV treatment (MV+*IGF-1*), and rats overexpressing both *IGF-1* and *FOXO1* with MV treatment (MV+*IGF-1*+*FOXO1*). Protein levels were measured by western blot or enzyme-linked immunosorbent assay (ELISA), and mRNA levels were detected by real-time reverse transcriptase-polymerase chain reaction (RT-qPCR). *IGF-1* and *FOXO1* expression were validated by detecting mRNA and protein levels. Diaphragmatic muscle contractility and morphometry were tested using stimulating electrodes in conjunction with hematoxylin and eosin (H&E) staining. Interleukin (IL)-6 and carbonylated protein were used for evaluating muscle atrophy and oxidation, respectively. Protein degradation was determined by troponin-I level and tyrosine release. Apoptosis was assessed using the terminal deoxynucleotidyl transferase-mediated uridine 5′-triphosphate (UTP) nick-end labeling (TUNEL) assay, alongside markers like Bax, B-cell lymphoma 2 (BCL-2), and Cleaved Caspase-3. Atrogin-1, muscle RING finger 1 (*MURF1*), neuronally expressed developmentally downregulated 4 (*NEDD4*), muscle ubiquitin ligase of SCF complex in atrophy-1 (*MUSA1*), and ubiquitinated protein was used to determine proteolysis. Additionally, protein synthesis was measured by assessing the rates of mixed muscle protein (MMP) and myosin heavy chain (MHC). Results: MV treatment caused *IGF-1* downregulation ($p < 0.01$) and *FOXO1* upregulation ($p < 0.01$). The *IGF-1* upregulation downregulated *FOXO1* in the MV+*IGF-1* group ($p < 0.001$) while *IGF-1* and *FOXO1* were both upregulated in the MV+*IGF-1*+FOXO1 group ($p < 0.001$). The treatment of MV decreased muscle contractility and cross-sectional areas of diaphragm muscle fibers ($p < 0.01$). Additionally, IL-6, troponin-1, tyrosine release, carbonylated protein, TUNEL positive nuclei, Bax, Cleaved Caspase-3, Atrogin-1, *MURF1*, neuronally expressed developmentally downregulated 4 (*NEDD4*), *MUSA1*, and ubiquitinated protein levels increased significantly in MV group ($p < 0.001$) while levels of BCL-2, fractional synthetic rate of MMP and MHC, and type I and type II MHC protein mRNA expression decreased in MV group ($p < 0.001$). All of these alterations were reversed in the MV+*IGF-1* group ($p < 0.01$), while the *IGF-1*-induced reversion was disrupted in the MV+*IGF-1*+*FOXO1* group ($p < 0.01$). Conclusions: *IGF-1* may protect diaphragmatic muscles from VIDD-induced structural damage and function loss by downregulating *FOXO1*. This action suppresses muscle breakdown and facilitates muscle remodeling in diaphragmatic muscles affected by VIDD.

Keywords: ventilator-induced diaphragmatic dysfunction; *IGF-1*; *FOXO1*; VIDD; skeletal muscle; diaphragm

Introduction

Mechanical ventilation (MV) is an important clinical tool for supporting or saving critically ill patients by providing adequate alveolar ventilation [1]. It has been reported that 40% of patients receive MV during critical illness and surgery [2]. In this context, MV is life-saving, however, prolonged MV can induce both lung and diaphragm impairment [3]. Ventilator-induced diaphragmatic dysfunction (VIDD) refers to the injury and weakness of diaphragmatic and inspiratory muscle fibers caused by MV [4] and is linked to exaggerated proteolysis and increased diaphragmatic oxidative stress [1,5]. Previous studies on both adult animal models and adult patients with acute respiratory failure have proven that the use of controlled MV (CMV) would result in an early decreased capacity of generating force [6,7]. Additional research found that 63% of patients who received prolonged MV suffered from VIDD [8]. Since diaphragm function is used to determine successful weaning from MV, and there is no effective treatment for VIDD [9,10], it is critical to explore therapy for treating VIDD and preventing increased mortality and morbidity induced by MV dependence.

Insulin-like growth factor (*IGF*)-*1* has been identified as a critical mediator for many beneficial physical processes like mitogenesis, cell survival, and development [11–13]. Furthermore, it has been shown that *IGF-1* plays a crucial role in modulating the size and function of skeletal muscle through mediating pathways of both protein synthesis and degradation [14]. Moreover, *IGF-1* has been proven to promote protein synthesis by activating the protein kinase B (AKT) pathway, a process that is typically reduced in conditions of muscle atrophy [15]. Alternatively, *IGF-1* may suppress protein synthesis by activating the myostatin pathway, a process that typically decreases conditions of muscle hypertrophy [16]. Previous studies have proven that the disruption of the IGF/AKT signaling pathway was responsible for protein synthesis downregulation in the diaphragm [17]. Moreover, *IGF-1* could also modulate protein degradation through the ubiquitin-proteasome system (UPS) [18,19] and autophagy [20]. Another key regulator of skeletal muscle atrophy is the forkhead box protein O1 (*FOXO1*) which regulates the expressions of genes associated with muscle atrophy [21]. It has been proven that *FOXO1* activation significantly promotes muscle atrophy while *FOXO1* inhibition protects against muscle atrophy [22]. Furthermore, *FOXO1* and *IGF-1* could regulate the muscle atrophy F-box (*MAFBX*)/*Artrogin-1* and muscle RING finger 1 (*MURF1*) that are E3 ubiquitin ligases in skeletal muscles which mediate protein polyubiquitination [23,24]. It should be noted that the *IGF-1*/AKT pathway could also mediate *FOXO* through mechanisms including the activation of IκB kinase β (IKKβ) which would induce muscle wasting when overexpressed in skeletal muscle. Additionally, previous data have shown that the *IGF-1*/AKT/FOXO pathways can inhibit autophagy [25].

Since VIDD is characterized by impaired muscle protein synthesis and increased muscle protein degradation [26], we hypothesized that *IGF-1* could be a viable target for VIDD treatment because of its capacity to normalize pathways associated with diaphragmatic muscle atrophy in VIDD. In the present study, we established rat models of VIDD by applying MV on rats and investigated the diaphragmatic alterations associated with different treatments on rats with different *IGF-1* expression levels, identifying the effect of *IGF-1* on skeletal muscle wasting and regeneration. Additionally, we also explored the role of *FOXO1* in the mechanism of *IGF-1* affecting the diaphragmatic muscle in VIDD by altering the expression of *FOXO1*. This study could elucidate how IGF-1 functions in treating diaphragmatic muscle affected by VIDD and the association of the underlying mechanism with *FOXO1*. By identifying potential treatment targets, this study aimed to establish effective and standard therapeutic strategies for treating VIDD.

Materials and Methods

Animals and Experimental Design

A total of 40 male Sprague-Dawley rats (4 months old, 250 $\pm$ 10 g) were obtained from Beijing Vital River Laboratory Animal Technology Co., Ltd. (Beijing, China) and housed individually at 37 °C. Before initiating the experiments, rats were maintained under standard 12-h light/dark cycles for one week with adequate food and water. Rats were randomly divided into 4 groups (n = 10/group) for subsequent experiments: normal rats with no MV treatment (NC), normal rats with MV treatment (MV), rats overexpressing *IGF-1* with MV treatment (MV+*IGF-1*), and rats overexpressing both *IGF-1* and *FOXO1* with MV treatment (MV+*IGF-1*+*FOXO1*). This experiment was approved by the Ethics Committee of Wuhan University (approval No. ZN2022034).

Overexpression of IGF-1 and FOXO1 by Adeno-Associated Virus (AAV)

The *IGF-1* AAV, *IGF-1*+*FOXO1* AAV, and control scramble AAV (with the promoter of CAG-mRuby2) were designed and constructed by GenePharma Corporation (Shanghai, China). The rats were anesthetized with a 0.3% sodium pentobarbital solution at a dosage of 0.2 mL/10 g and all AAV delivered to rats was standardized at a titer of 1×10^{13} vector genomes (vg)/mL. The delivery was performed with a microsyringe (87900, Hamilton, Shanghai, China) and AAV was injected into the right ventricle. Rats in the control and MV groups were injected with control scramble AAV (1×10^{12} vg/mouse) while rats in the MV+*IGF-1* group were injected with *IGF-1* AAV (1×10^{12} vg/mouse), and rats in the MV+*IGF-1*+*FOXO1* group were injected with *IGF-1*+*FOXO1* AAV (1×10^{12} vg/mouse). During the delivery, the needle was fixed within the rats'

bodies for 5 min before being slowly removed. The AAV injection was administered at a rate of 0.5 µL/min. Subsequent experiments would begin two weeks after the AAV injection.

Mechanical Ventilation Treatment

All surgery procedures of MV treatment were performed under aseptic conditions and using aseptic techniques. Rats were anesthetized via intraperitoneal injection of sodium pentobarbital (40 mg/kg; P3761, Sigma-Aldrich, St. Louis, MO, USA). Prior to anesthesia and every two hours afterward, rats received glycopyrrolate (0.04 mg/kg) via intramuscular injection. Subsequently, rats were tracheostomized and received MV with O_2-enriched humidified air at 37 °C using a volume-cycles ventilator (SAR-830/AP, Quatronix, Beijing, China) for 18 h. MV tidal volume and respiratory rate were set as 5 mL/kg of body weight and 50 to 60 breaths/minute, respectively. The positive end-expiratory pressure was 1 cm H_2O. For the last 6 h of the MV treatment, the jugular vein was cannulated to infuse saline, sodium pentobarbital (5 mg/kg/h), and [^{13}C] leucine. Rats in the NC group were anesthetized without MV treatment or [^{13}C] leucine infusion. Throughout the surgery period, rats received enteral nutrition through a nasogastric tube, and received continuous care and monitoring while maintained at 37 $\pm$ 1 °C.

Sample Collection

At 24 h post-surgery, rats were euthanatized using 180 mg/kg sodium pentobarbital via intraperitoneal injection, and euthanasia depth was assessed via pedal and blink reflexes. Subsequently, the arterial blood was obtained for subsequent use and the diaphragm was collected from all rats. Costal diaphragm segments were used for assessing contractility, while a fragment was frozen in liquid nitrogen and subsequently stored at –80 °C. The remaining diaphragm was preserved in an alcohol-formol bath and subsequently embedded in paraffin. Frozen tissues underwent molecular expression analyses while the paraffin-embedded tissues were subject to histological observations.

Diaphragm Contractility Test

Diaphragm muscle bundle contractility was measured *in vitro* at 37 °C using a temperature-controlled organ bath and a stimulating electrode. Muscle bundles were stimulated with a frequency of 160 Hz to establish the optimal muscle length (L_0) for the peak twitch force, which was then measured. Subsequently, twitch characteristics were measured at L_0via a single twitch stimulation at 1 Hz. In addition, the maximal tetanic force was obtained by stimulating the muscle bundle twice at 160 Hz for 250 ms with a 2-minute interval. Muscle force was normalized for the cross-sectional areas of the bundles, calculated as the bundle weight divided by muscle L_0 and specific density.

Muscle Morphometry

Muscle morphometry was assessed using hematoxylin and eosin (H&E) staining. The paraffin-embedded diaphragm tissues were cut into 8-µm sections and stained with hematoxylin (H3136, Sigma-Aldrich, Saint Louis, MO, USA) and eosin (E4009, Sigma-Aldrich, Saint Louis, MO, USA). After being dehydrated and sealed, the diaphragmatic muscle fiber phenotype and morphometry were observed under a light microscope (Olympus CK31, Olympus, Tokyo, Japan). Cross-sectional areas were measured and adjusted for shortening by dividing the cross-sectional area with 1.53 (the specific correction factor for the diaphragm).

Enzyme-Linked Immunosorbent Assay (ELISA)

Troponin-I levels in skeletal muscles and interleukin (IL)-6 protein levels in plasma and diaphragm muscles were quantified using dedicated sandwich ELISA kits (troponin-I: ab246529, Abcam, Cambridge, MA, USA; IL-6: PI326, Beyotime, Shanghai, China) across various groups.

Tyrosine Release

The rate of free tyrosine release from tissue proteins was measured to assess protein degradation and catabolism. Tyrosine was measured using the fluorometric method, in which muscles were homogenized in 10% (w/v) trichloroacetic acid and centrifugated. The supernatants were collected and assayed for tyrosine.

Terminal Deoxynucleotidyl Transferase-Mediated Uridine 5′-Triphosphate (UTP) Nick-End Labeling (TUNEL) Assay

Apoptotic nuclei within paraffin-embedded diaphragm sections were identified using the TUNEL assay kit (C1088, Beyotime, Shanghai, China) according to the manufacturer's instructions. After two phosphate-buffered saline (PBS) washes, cells were stained with 4',6-diamidino-2-phenylindole (DAPI; C1005, Beyotime, Shanghai, China). Subsequently, the stained cells were visualized under a fluorescence microscope (CKX53, Olympus, Tokyo, Japan) to quantify apoptotic cells. The mean count of TUNEL-positive cells was calculated from three selected microscopic regions for each diaphragm sample.

Protein Synthesis

The fractional synthesis rate of a specific protein was measured by dividing the [^{13}C] leucine enrichment in the protein by the magnitude of [^{13}C] leucine enriched in the precursor pools, determined via [^{13}C] leucine analysis in plasma or tissue fluid. Mixed muscle protein (MMP) and myosin heavy chain (MHC) proteins were isolated from the diaphragm and the magnitudes of [^{13}C] leucine enriched in them were quantified. Rates of MMP and MHC protein synthesis were obtained based on their corresponding precursor pools.

Table 1. Primer sequences.

Name	Sequences (5′-3′)
IGF-1-F	CAGCAGTCTTCCAACCCAAT
IGF-1-R	CCACACACGAACTGAAGAGC
FOXO1-F	AAGAGCGTGCCCTACTTCAA
FOXO1-R	TTCCTTCATTCTGCACACGA
Atrogin-1-F	TACTAAGGAGCGCCATGGATACT
Atrogin-1-R	GTTGAATCTTCTGGAATCCAGGAT
MURF1-F	TGACCAAGGAAAACAGCCACCAG
MURF1-R	TCACTCCTTCTTCTCGTCCAGGATGG
NEDD4-F	TTGCAGCAACAACAAGAACC
NEDD4-R	TAGGTTGTCCTGAGGGGTTG
MUSA1-F	GTGATCATGCCAATCCACAG
MUSA1-R	CATGAATGTCACCATGCACA
Type II *MHC*-F	GCGGTGACGCCGCAGGGGCA
Type II *MHC*-R	TGTATGCACACCGTGTCCAA
Type I *MHC*-F	GGGTCTCACACCTACCAGGT
Type I *MHC*-R	CGCCCTCCAGGTAGGTTCTGTGCTG
GAPDH-F	CCACACACGAACTGAAGAGC
GAPDH-R	GCTGTAGCCAAATCGTTGT

IGF, insulin-like growth factor; *FOXO1*, forkhead box protein O1; *MURF1*, muscle RING finger 1; *NEDD4*, neuronally expressed developmentally downregulated 4; *MUSA1*, muscle ubiquitin ligase of SCF complex in atrophy-1; *MHC*, myosin heavy chain; *GAPDH*, glyceraldehyde-3-phosphate dehydrogenase; F, forward; R, reverse.

Real-Time Reverse Transcriptase-Polymerase Chain Reaction (RT-qPCR)

RNA extraction utilized TRIzol® (DP424, Tiangen, Beijing, China) followed by centrifugation at 12,000 ×g. RNA purity (OD 260 nm/OD 280 nm = 1.8–2.2) was assessed using a full-wavelength spectrophotometer (OSE-260, Tiangen, Beijing, China). Reverse transcription from RNA to cDNA occurred using FastQuant cDNA (KR116, Tiangen, Beijing, China) according to the manufacturer's instructions. RT-qPCR was conducted using the LightCycler96 fluorescence quantitative instrument for PCR (Roche, Shanghai, China) with a defined thermal cycling program. Relative expression levels were normalized to those of human *GAPDH* and $2^{-\Delta\Delta Cq}$ was used for analyzing the data. Table 1 lists the primer sequences used in RT-qPCR.

Western Blot

Total proteins were collected by using radioimmunoprecipitation assay (RIPA) lysis buffer (P0013J, Beyotime Biotechnology Co., Ltd., Shanghai, China) containing complete proteinase inhibitor cocktail (PMSF; ST506, Beyotime Biotechnology Co., Ltd., Shanghai, China) and quantified using a bicinchoninic acid (BCA) assay kit (P0010S, Beyotime Biotechnology Co., Ltd., Shanghai, China). After adding the protein loading buffer (P0015, Beyotime Biotechnology Co., Ltd., Shanghai, China), proteins were denatured in 100 °C hot water for 5–10 min for the subsequent sodium dodecyl-sulfate polyacrylamide gel electrophoresis (SDS-PAGE) electrophoresis. Subsequently, proteins were transferred to the polyvinylidene fluoride (PVDF) membrane (IPVH00010, Millipore Sigma, Billerica, MA, USA) with an electric current of 250 mA for 1.5 h. Then, the membrane was blocked with skim milk (G5002, Serveicebio, Wuhan, China) for 1 h at room temperature, followed by incubation with primary antibodies (IGF-1: 1:1000 dilution, ab133542, Abcam, Cambridge, MA, USA; FOXO1: 1:1000 dilution, ab179450, Abcam, Cambridge, MA, USA; Bax: 1:1000 dilution, ab182734, Abcam, Cambridge, MA, USA; B-cell lymphoma 2 (BCL-2): 1:2000 dilution, ab182858, Abcam, Cambridge, MA, USA; Cleaved Caspase-3: 1:500 dilution, ab2302, Abcam, Cambridge, MA, USA; MMP: 1:1000 dilution, ab51075, Abcam, Cambridge, MA, USA; MHC: 1:1000 dilution, ab37484, Abcam, Cambridge, MA, USA; Ubiquitin: 1:1000 dilution, ab134953, Abcam, Cambridge, MA, USA; Carbonyl: 1:1000 dilution, ab178020, Abcam, Cambridge, MA, USA; ACTIN: 1:500 dilution, ab8226, Abcam, Cambridge, MA, USA) at 4 °C overnight. The membranes were washed with tris buffered saline with tween (TBST; AR0144, Boster Bio, Wuhan, China) three times for 10 minutes each and incubated with the secondary antibodies (horseradish peroxidase-labeled goat anti-mouse IgG: 1:2000 dilution, Cat. No. ZB-2305, ZSGB; horseradish peroxidase-labeled goat anti-rabbit IgG: 1:2000 dilution, Cat. No. ZB-2301, ZSGB) for 1 h at room temperature. After washing membranes, the antibody-reactive bands were revealed by enhanced chemiluminescence (Tanon-1600, Shanghai Tanon Life Science Co., Ltd., Shanghai, China) and exposed on radiographic film. The images were processed by Adobe PhotoShop CS3 (Adobe Systems Incorporated, San Jose, CA, USA) while the gray analysis was performed by AlphaEaseFC 4.0 (Alpha Innotech. San Leandro, CA, USA).

Statistical Analysis

All data obtained from repeat experiments were analyzed by GraphPad Prism 8.0.2 (GraphPad Software Inc., San Diego, CA, USA) and expressed as means ± standard deviation (SD). Differences between groups were analyzed using the Analysis of Variance (ANOVA) test coupled with post hoc 'all pairwise' comparisons. Statistical significance was considered when $p < 0.05$.

Results

IGF-1 Plays Roles in VIDD and Mediates FOXO1 Expression

The mRNA and protein levels are shown in Fig. 1A,B, respectively. *IGF-1* was downregulated ($p < 0.01$) and *FOXO1* was upregulated in rats treated with MV ($p < 0.01$), verifying the association of *IGF-1* and *FOXO1* with MV-induced VIDD. In the MV+*IGF-1* group, significant over-

expression of *IGF-1* ($p < 0.001$) confirmed the successful creation of rats with heightened *IGF-1* levels. This overexpression corresponded with a notable downregulation of *FOXO1* ($p < 0.001$), indicating *IGF-1*'s regulatory influence on *FOXO1*. In the MV+*IGF-1*+*FOXO1* group, the level of *IGF-1* was equally as high as the MV+*IGF-1* group ($p > 0.05$) while the *FOXO1* levels were successfully upregulated compared to the MV+*IGF-1* group ($p < 0.001$).

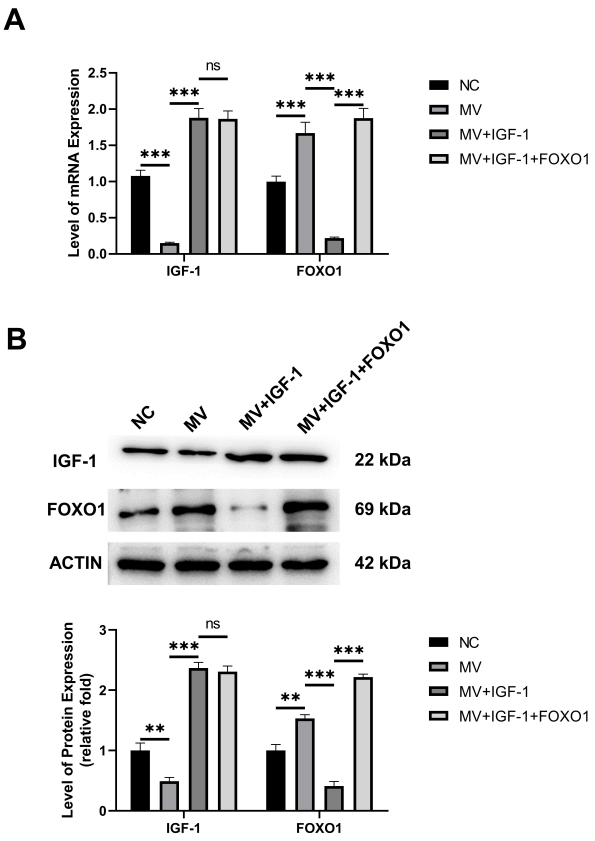

Fig. 1. *IGF-1* plays roles in ventilator-induced diaphragmatic dysfunction (VIDD) and mediates *FOXO1* expression. (A) The mRNA expressions of *IGF-1* and *FOXO1* in differently treated rat models were identified by real-time reverse transcriptase-polymerase chain reaction (RT-qPCR). (B) The protein expressions of *IGF-1* and *FOXO1* in differently treated rat models were identified by western blot. N = 10. $^{**}p < 0.01$, $^{***}p < 0.001$, ns, No Significance ($p > 0.05$).

The Effect of IGF-1 Mediating FOXO1 on Muscle Structure and Injury in VIDD

As shown in Fig. 2A, MV treatment significantly reduced the capacity of diaphragm generating force ($p < 0.01$), which was mitigated ($p < 0.001$) in the MV+*IGF-1* group. While this upregulating *FOXO1* in the MV+*IGF-1*+*FOXO1* group nullified this remedy ($p < 0.001$). Similarly, as shown in Fig. 2B, *IGF-1* could reverse the decreased diaphragm cross-sectional areas ($p < 0.001$) which would also be decreased by upregulated expression of *FOXO1* ($p < 0.01$). Fig. 2C shows increased interleukin (IL)-6 protein levels in diaphragm muscles due to MV treatment ($p < 0.001$), indicating more muscle atrophy. Upregulating *IGF-1* decreased IL-6 levels ($p < 0.001$), mitigating atrophy, while increased *FOXO1* elevated the level of IL-6 ($p < 0.001$) and subsequent atrophy. Moreover, the levels of troponin-I and free tyrosine release shown in Fig. 3A,B, respectively, verified that MV-induced VIDD would increase muscle protein degradation which was represented by increased levels of troponin-I and free tyrosine release ($p < 0.001$). The levels of troponin-I and free tyrosine release ($p < 0.001$) decreased in the MV+*IGF-1* group, inhibiting protein degradation. Contrarily, increasing *FOXO1* would reverse the decreased troponin-I and free tyrosine release levels ($p < 0.001$) and inhibit protein degradation. In addition, the levels of protein carbonylation that represent the oxidative stress of muscles are shown in Fig. 3C, demonstrating that *IGF-1* could decrease the level of protein carbonylation ($p < 0.001$), thus possessing the effect of suppressing muscle oxidation. Additionally, increased *FOXO1* could reverse the decreased level of protein carbonylation ($p < 0.001$).

The Effect of IGF-1 Mediating FOXO1 on Apoptosis in Diaphragm Muscles

Fig. 4A,B display TUNEL assay results, indicating increased TUNEL positive nuclei due to MV treatment ($p < 0.001$), a trend reversed by *IGF-1* ($p < 0.01$). This illustrates that *IGF-1* counters VIDD-induced apoptosis in diaphragm muscles. Conversely, upregulation of *FOXO1* increased TUNEL-positive nuclei, signifying elevated apoptosis ($p < 0.001$). The same effect of *IGF-1* mediating *FOXO1* on apoptosis was revealed by the western blot as shown in Fig. 4C,D. The protein levels of Bax and Cleaved Caspase-3 increased ($p < 0.001$) while the level of BCL-2 decreased ($p < 0.001$) in the MV group, which were all reversed by the *IGF-1* overexpression in MV+*IGF-1* group ($p < 0.001$). However, these alterations were opposite in the MV+*IGF-1*+*FOXO1* group ($p < 0.001$), indicating *FOXO1*'s counteractive effect on *IGF-1*'s mediation of apoptosis.

The Effect of IGF-1 Mediating FOXO1 on Proteolysis

The proteolysis associated with the ubiquitin-proteasome pathway was evaluated by measuring related markers shown in Fig. 5, in which Atrogin-1, *MURF1*, *NEDD4* and muscle ubiquitin ligase of SCF complex in atrophy-1 (*MUSA1*) are important regulators of ubiquitin-mediated protein degradation in skeletal muscle. Through RT-qPCR, levels of Atrogin-1 (Fig. 5A), *MURF1* (Fig. 5B), *NEDD4* (Fig. 5C) and *MUSA1* (Fig. 5D) were found upregulated following MV treatment ($p < 0.001$), while

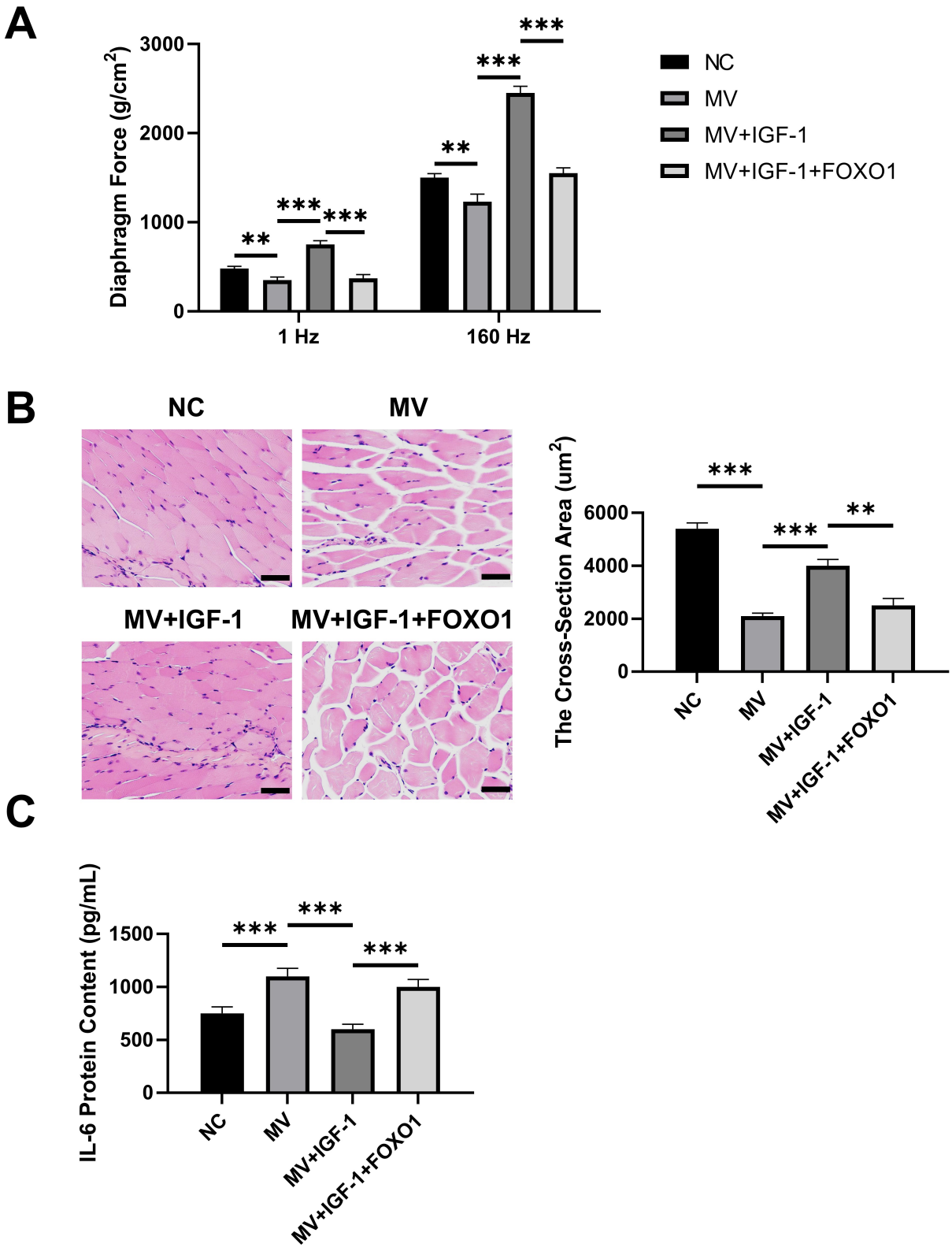

Fig. 2. The effect of *IGF-1* mediating *FOXO1* on muscle structure and injury in VIDD. (A) The peak diaphragm force generated in response to stimulation of 1 and 160 Hz in differently treated rat models. (B) The representative images and quantification of cross-sectional areas of diaphragm muscle fibers in each group (scale bar: 50 μm). (C) The interleukin (IL)-6 protein levels in diaphragm muscles from differently treated rats. N = 10. $^{**}p < 0.01$, $^{***}p < 0.001$.

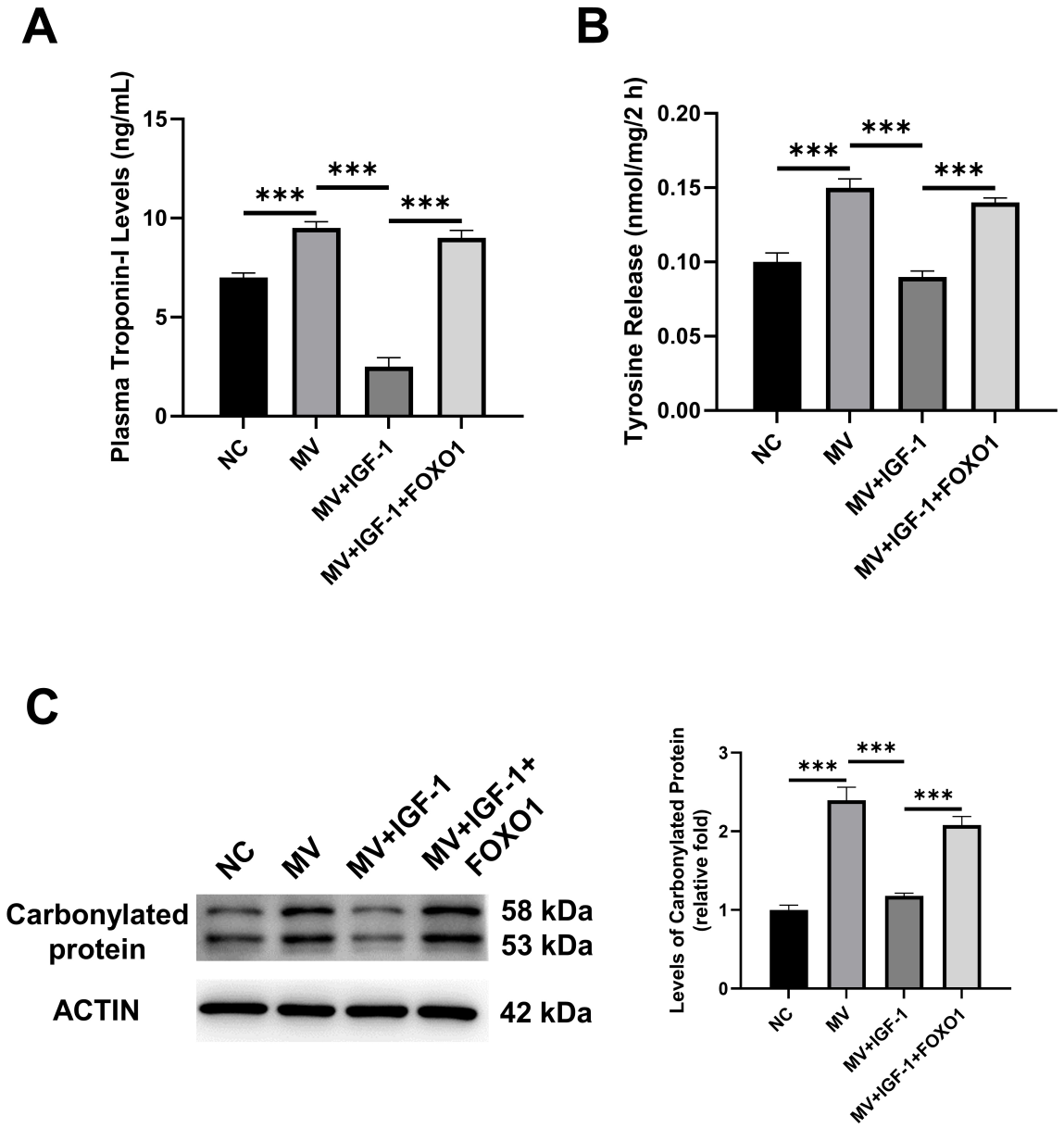

Fig. 3. The effect of *IGF-1* mediating *FOXO1* on muscle structure and injury in VIDD. (A) The levels of troponin-I in plasma from differently treated rats. (B) The free tyrosine release from differently treated rats. (C) The representative western blotting images and quantification of carbonylated protein levels in diaphragm muscles from differently treated rats. N = 10. ***$p < 0.001$.

the upregulations were reversed by *IGF-1* overexpression ($p < 0.01$). Moreover, the lowered mRNA expressions increased again after *FOXO1* upregulation ($p < 0.001$). The western blot results were shown in Fig. 5E and demonstrated a similar trend in *IGF-1* and *FOXO1* regulation of ubiquitinated protein. Protein ubiquitination increased in the MV group ($p < 0.001$), decreased in the MV+*IGF-1* group ($p < 0.01$), and increased again in the MV+*IGF-1*+*FOXO1* group ($p < 0.01$).

The Effect of IGF-1 Mediating FOXO1 on Protein Synthesis in the Diaphragm

The mixed muscle protein (MMP) synthesis and myosin heavy chain (MHC) protein synthesis represented overall muscle protein synthesis and contractile protein synthesis, respectively. As shown in Fig. 6A,B, MV slowed the fractional synthesis of both MMP and the MHC protein ($p < 0.001$) in the MV group while *IGF-1* overexpression increased the fractional synthesis of both MMP and the MHC protein ($p < 0.001$) in the MV+*IGF-1* group. In the MV+*IGF-1*+*FOXO1* group where *IGF-1* and *FOXO1* were both upregulated, the fractional synthesis of both MMP and

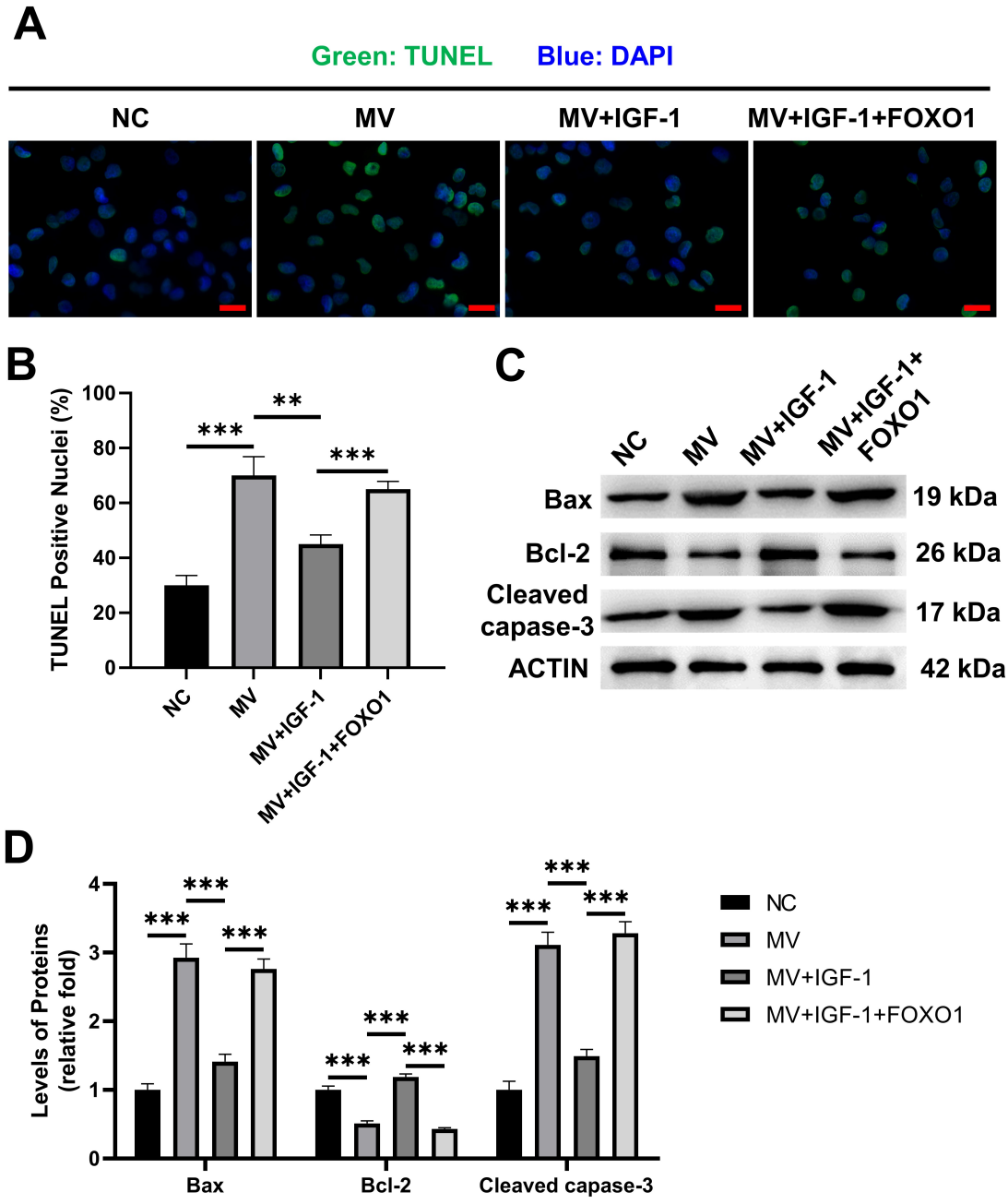

Fig. 4. The effect of *IGF-1* mediating *FOXO1* on apoptosis in diaphragm muscles. (A) Representative images of terminal deoxynucleotidyl transferase-mediated uridine 5′-triphosphate (UTP) nick-end labeling (TUNEL) assay performed on diaphragms from differently treated rats. Scale bar = 50 µm. (B) The quantification of positively stained nuclei in the TUNEL assay for diaphragms. (C) The representative western blotting images and (D) the quantification of protein levels of Bax, B-cell lymphoma 2 (BCL-2), and Cleaved Caspase-3. N = 10. $^{**}p < 0.01$, $^{***}p < 0.001$.

the MHC protein decreased ($p < 0.01$). Furthermore, the mRNA levels of both type I and type II (Fig. 6C,D) were lowered in the MV group ($p < 0.001$), which was reversed in the MV+*IGF-1* group ($p < 0.001$). When the *FOXO1* was also upregulated in the MV+*IGF-1*+*FOXO1* group, the mRNA levels of both type I and type II were lowered again ($p < 0.001$).

Discussion

This study confirmed the hypothesis that *IGF-1* could contribute to the recovery of diaphragmatic skeletal muscles after VIDD-induced muscle atrophy. Meanwhile, we also identified the underlying mechanism was associated with the level of *IGF-1*-mediated *FOXO1*, increased muscle contractility and decreased fiber atrophy.

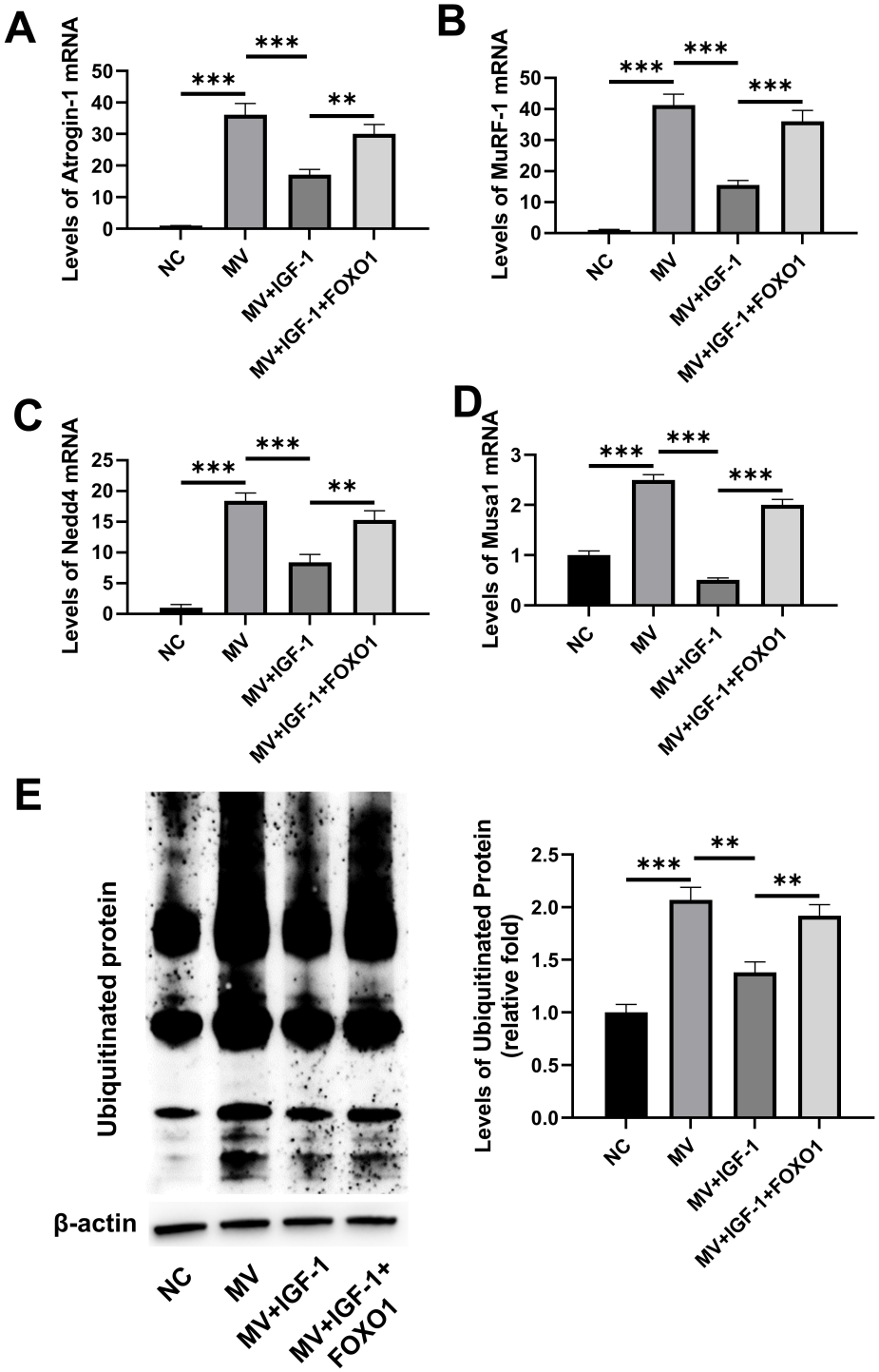

Fig. 5. The effect of *IGF-1* mediating *FOXO1* on proteolysis. The mRNA expression levels of (A) Atrogin-1, (B) *MURF1*, (C) *NEDD4*, and (D) *MUSA1* in diaphragms from differently treated rats. (E) The representative western blotting images and quantification of ubiquitinated protein levels in diaphragms from differently treated rats. N = 10. $^{**}p < 0.01$, $^{***}p < 0.001$.

This study has shown that MV treatment induced muscle contractile dysfunction and a significant decrease in myofiber cross-sectional area, resulting in limited pulmonary function [27]. However, these disruptions of diaphragm function were mitigated by *IGF-1* upregulation. VIDD is characterized by decreased diaphragm contractile force and muscle fiber atrophy [28], indicating the potential benefits of *IGF-1* in VIDD recovery. Importantly, markers of muscle damage and protein degradation decreased in MV-treated rats with *IGF-1* upregulation followed by *FOXO1* downregulation. Conversely, upregulating *FOXO1* increased these values in rats. Troponin-I has

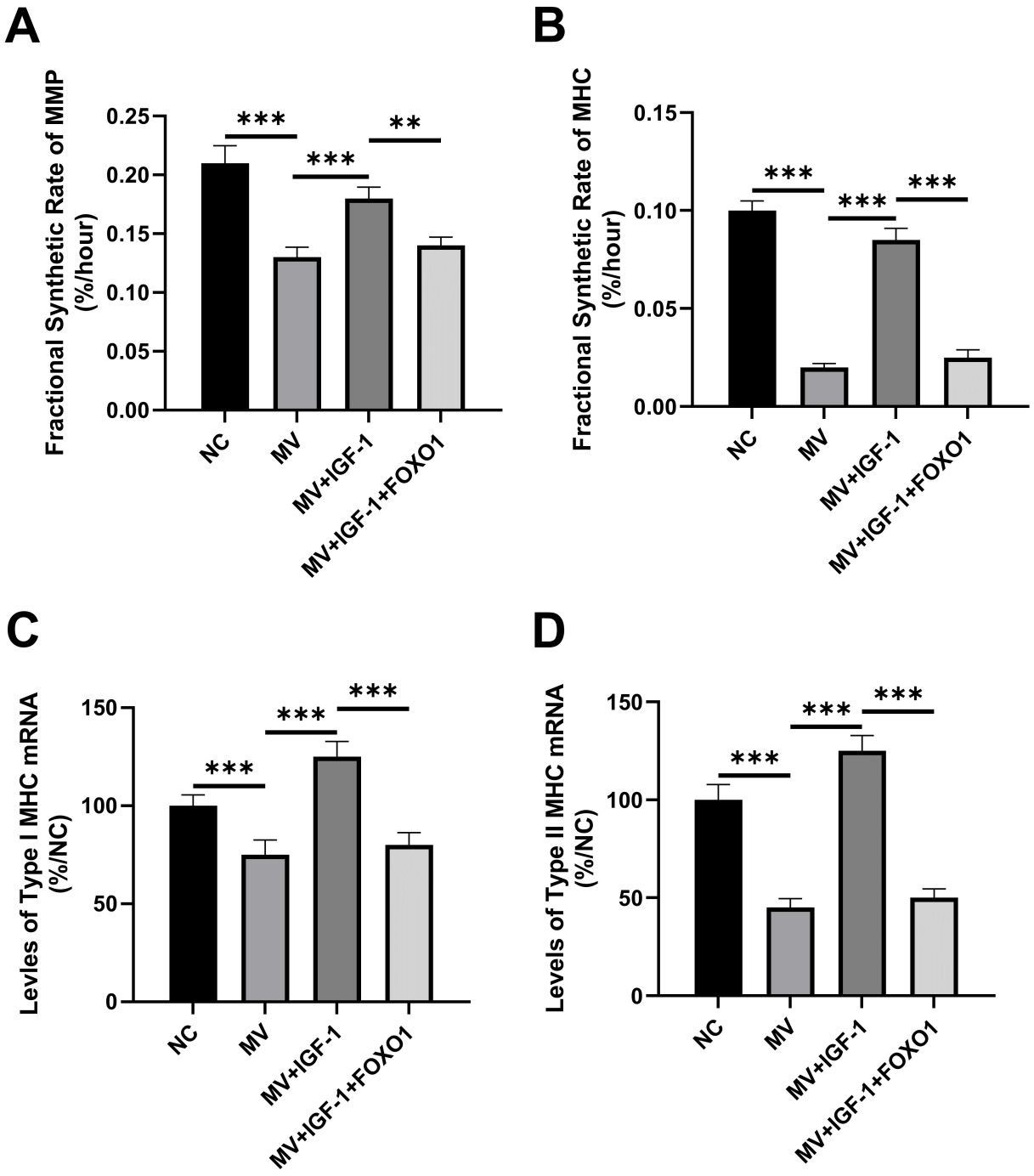

Fig. 6. The effect of *IGF-1* mediating *FOXO1* on protein synthesis in the diaphragm. The fractional synthetic rates of (A) mixed muscle protein (MMP) and (B) myosin heavy chain (MHC) protein obtained by calculations in which the [^{13}C] leucine was used as a surrogate measure of the tissue fluid [^{13}C] leucine-tRNA precursor pool. mRNA levels of (C) type I *MHC* and (D) type II *MHC* in the diaphragms from differently treated groups. N = 10. $^{**}p < 0.01$, $^{***}p < 0.001$.

been proven to be essential to regulating striated muscle contraction [29] and has been proposed as a sensitive and fast marker for evaluating skeletal muscle damage and proteolysis [30]. As previously reported, IL-6 was upregulated in the skeletal muscles of immobilized rats and mice with IL-6 deficiency were protected from immobility-induced muscle atrophy [31,32], making the increased level of IL-6 a marker for increased muscle atrophy. Furthermore, increased *IGF-1* levels reduced tyrosine release and carbonylated protein, highlighting IGF-1's role in diminishing protein degradation and oxidative stress in the diaphragm's skeletal muscle.

In this study, *IGF-1* upregulation was accompanied by the elimination of *FOXO1* in the diaphragm, leading to decreased proteasome activity markers including protein ubiquitination, Atrogin-1, *MURF1*, *NEDD4*, and *MUSA1*. Conversely, disrupting *FOXO1* downregulation reversed the decreased muscle proteolysis. These findings suggest that *IGF-1* affects skeletal muscle proteolysis in the diaphragm by downregulating *FOXO1*. This is plausible as *FOXO* modulation by reactive oxygen species [33] and MV-induced diaphragm redox dependency [1,34] have been reported. *MUSA1* has been associated with sepsis or inhibited bone morphogenic protein signaling, leading to muscle atrophy [35]. Therefore, the decreased *MUSA1* induced by *IGF-1* overexpression and *FOXO1* downregulation demonstrated the effects of *IGF-1* on preventing muscle atrophy, and the underlying mechanism might also be associated with bone morphogenesis. Additionally, repeated evidence suggests that apoptosis significantly contributes to skeletal muscle atrophy [36,37] and the activation of apoptosis has been proven to be responsible for the development of VIDD [38]. *IGF-1* mitigated MV-induced apoptosis, aligning with its effect on reducing MV-induced proteolysis, as apoptosis signaling significantly contributes to proteolytic degradation and skeletal muscle atrophy [39]. *Caspase*-dependent apoptosis is prevalent in the atrophic diaphragm induced by various conditions. MV-induced atrophy can be alleviated by inhibiting caspase-dependent apoptosis [40]. The activated apoptosis signaling would activate caspase-3, whose degradation would be further facilitated by cleaving actomyosin through the ubiquitin-proteasome pathway during proteolysis [41]. Furthermore, Bax and BCL-2 were proven to regulate apoptosis by modulating caspases [42]. The findings show that the series of MV-induced reactions of apoptosis and proteolysis could be reversed by *IGF-1* while rebounded by *FOXO1* roundly, which proves that *IGF-1* has effects on preventing diaphragmatic muscle atrophy in VIDD via FOXO1 downregulation.

Since muscle mass wasting and muscle protein are associated with the imbalance of protein synthesis and breakdown [43,44], the rehabilitation of skeletal muscle after VIDD would be promoted by increased protein synthesis. The synthesis of MMP in a muscle sample represents the average synthetic rate of all proteins [45], while HMC, which is essential for contractile apparatus in muscles, constitutes approximately 25% of skeletal muscle mass [46]. This study found decreased MMP synthetic rates induced by MV, indicating reduced protein synthesis in the diaphragm when unloaded [47]. Conversely, increased type I and type II *MHC* isoforms mRNA expressions have been found in people after resistance exercise [48], suggesting that the increased type I and type II *MHC* isoforms mRNA expressions and the MHC protein synthesis are related to the recovery of muscle fiber size and muscle remodeling [49]. Furthermore, mRNAs encode type I MHC protein and type II MHC protein representing 26% and 41% of MHC protein in the diaphragm of rats, respectively [50]. Therefore, in this study, type I *MHC* mRNA and type II *MHC* mRNA were measured to verify the association between protein synthesis and *MHC* mRNA. The improved levels of protein syntheses, type I *MHC* mRNA, and type II *MHC* mRNA caused by *IGF-1* and reversed by upregulating *FOXO1*, verifying that *IGF-1* could promote protein synthesis in the diaphragm by inhibiting *FOXO1* expression.

The collective findings described and discussed above confirm *IGF-1*'s positive impact on diaphragmatic skeletal muscle recovery from VIDD. *IGF-1* increases muscle contractility, optimizes fiber structure, mitigates protein degradation, apoptosis and proteolysis, and promotes protein synthesis in the diaphragm. While *IGF-1* was found to downregulate *FOXO1*, if the downregulation of *FOXO1* was unsuccessful, the promotion of muscle rehabilitation would be unsuccessful, demonstrating the significance of *FOXO1* in the mechanism of *IGF-1* facilitating skeletal muscle remodeling after VIDD.

Conclusions

By downregulating *FOXO1*, *IGF-1* was proven to be effective in ameliorating protein degradation and promoting protein synthesis in the diaphragm after VIDD-induced atrophy and muscle wasting. The findings in this study extend the understating of the mechanism of skeletal muscle remodeling and rehabilitation, and indicate *IGF-1* and *FOXO1* as potential targets for VIDD treatment.

Availability of Data and Materials

The datasets used and/or analyzed during the current study are available from the corresponding authors upon reasonable request.

Author Contributions

LY and XJ contributed to the study concept and design. SF, JT, and WD contributed to the acquisition of data. YZ and LY performed the statistical analysis. XJ was involved in the interpretation of the data. All authors contributed to editorial changes in the manuscript. All authors read and approved the final manuscript. All authors have participated sufficiently in the work to take public responsibility for appropriate portions of the content and agreed to be accountable for all aspects of the work in ensuring that questions related to its accuracy or integrity.

Ethics Approval and Consent to Participate

This experiment was approved by the Ethics Committee of Wuhan University (approval No. ZN2022034).

Acknowledgment

Not applicable.

Funding

This research was funded by Wuhan Science and Technology Bureau knowledge innovation project (No: 2023020201010191); Hubei Province health and family planning scientific research project (No: WJ2023F046).

Conflict of Interest

The authors declare no conflict of interest.

References

[1] Yoshihara T, Deminice R, Hyatt HW, Ozdemir M, Nguyen BL, Powers SK. Angiotensin 1-7 protects against ventilator-induced diaphragm dysfunction. Clinical and Translational Science. 2021; 14: 1512–1523.

[2] Wunsch H, Wagner J, Herlim M, Chong DH, Kramer AA, Halpern SD. ICU occupancy and mechanical ventilator use in the United States. Critical Care Medicine. 2013; 41: 2712–2719.

[3] Zambelli V, Murphy EJ, Delvecchio P, Rizzi L, Fumagalli R, Rezoagli E, *et al*. Treatment with levosimendan in an experimental model of early ventilator-induced diaphragmatic dysfunction. Drug Target Insights. 2023; 17: 39–44.

[4] Ichinoseki-Sekine N, Smuder AJ, Morton AB, Hinkley JM, Mor Huertas A, Powers SK. Hydrogen sulfide donor protects against mechanical ventilation-induced atrophy and contractile dysfunction in the rat diaphragm. Clinical and Translational Science. 2021; 14: 2139–2145.

[5] Dridi H, Yehya M, Barsotti R, Reiken S, Angebault C, Jung B, *et al*. Mitochondrial oxidative stress induces leaky ryanodine receptor during mechanical ventilation. Free Radical Biology & Medicine. 2020; 146: 383–391.

[6] Koopman AA, de Jager P, Blokpoel RGT, Kneyber MCJ. Ventilator-induced lung injury in children: a reality? Annals of Translational Medicine. 2019; 7: 506.

[7] Liang F, Emeriaud G, Rassier DE, Shang D, Gusev E, Hussain SNA, *et al*. Mechanical ventilation causes diaphragm dysfunction in newborn lambs. Critical Care (London, England). 2019; 23: 123.

[8] Zambelli V, Sigurtà A, Rizzi L, Zucca L, Delvecchio P, Bresciani E, *et al*. Angiotensin-(1-7) exerts a protective action in a rat model of ventilator-induced diaphragmatic dysfunction. Intensive Care Medicine Experimental. 2019; 7: 8.

[9] Karageorgos V, Proklou A, Vaporidi K. Lung and diaphragm protective ventilation: a synthesis of recent data. Expert Review of Respiratory Medicine. 2022; 16: 375–390.

[10] Spiesshoefer J, Kersten A, Enriquez Geppert J, Regmi B, Senol M, Kabitz HJ, *et al*. State-of-the-Art Opinion Article on Ventilator-Induced Diaphragm Dysfunction: Update on Diagnosis, Clinical Course, and Future Treatment Options. Respiration; International Review of Thoracic Diseases. 2023; 102: 74–82.

[11] Józefiak A, Larska M, Pomorska-Mól M, Ruszkowski JJ. The IGF-1 Signaling Pathway in Viral Infections. Viruses. 2021; 13: 1488.

[12] Bhalla S, Mehan S, Khan A, Rehman MU. Protective role of IGF-1 and GLP-1 signaling activation in neurological dysfunctions. Neuroscience and Biobehavioral Reviews. 2022; 142: 104896.

[13] Hanwright PJ, Qiu C, Rath J, Zhou Y, von Guionneau N, Sarhane KA, *et al*. Sustained IGF-1 delivery ameliorates effects of chronic denervation and improves functional recovery after peripheral nerve injury and repair. Biomaterials. 2022; 280: 121244.

[14] Feng L, Li B, Xi Y, Cai M, Tian Z. Aerobic exercise and resistance exercise alleviate skeletal muscle atrophy through IGF-1/IGF-1R-PI3K/Akt pathway in mice with myocardial infarction. American Journal of Physiology. Cell Physiology. 2022; 322: C164–C176.

[15] Yoshida T, Delafontaine P. Mechanisms of IGF-1-Mediated Regulation of Skeletal Muscle Hypertrophy and Atrophy. Cells. 2020; 9: 1970.

[16] Bataille S, Chauveau P, Fouque D, Aparicio M, Koppe L. Myostatin and muscle atrophy during chronic kidney disease. Nephrology, Dialysis, Transplantation: Official Publication of the European Dialysis and Transplant Association - European Renal Association. 2021; 36: 1986–1993.

[17] Jaiswal N, Gavin M, Loro E, Sostre-Colón J, Roberson PA, Uehara K, *et al*. AKT controls protein synthesis and oxidative metabolism via combined mTORC1 and FOXO1 signalling to govern muscle physiology. Journal of Cachexia, Sarcopenia and Muscle. 2022; 13: 495–514.

[18] Xia H, Zhang B, Yang D, Zhu C, Zhang J, Chen H, *et al*. Yi-Qi-Jian-Pi-Xiao-Yu-Xie-Zhuo Formula Improves Muscle Atrophy via Modulating the IGF-1/PI3K/Akt Signaling Pathway in 5/6 Nephrectomized Rats. Frontiers in Pharmacology. 2021; 12: 624303.

[19] Chen X, Pang Z, Wang Y, Zhu L, Liu J, Du J. Cezanne contributes to cancer progression by playing a key role in the deubiquitination of IGF-1R. American Journal of Cancer Research. 2020; 10: 4342–4356.

[20] Angulo J, El Assar M, Álvarez-Bustos A, Rodríguez-Mañas L. Physical activity and exercise: Strategies to manage frailty. Redox Biology. 2020; 35: 101513.

[21] Li Z, Liu C, Li S, Li T, Li Y, Wang N, *et al*. BMSC-Derived Exosomes Inhibit Dexamethasone-Induced Muscle Atrophy *via* the miR-486-5p/FoxO1 Axis. Frontiers in Endocrinology. 2021; 12: 681267.

[22] Oyabu M, Takigawa K, Mizutani S, Hatazawa Y, Fujita M, Ohira Y, *et al*. FOXO1 cooperates with C/EBPδ and ATF4 to regulate skeletal muscle atrophy transcriptional program during fasting. FASEB Journal: Official Publication of the Federation of American Societies for Experimental Biology. 2022; 36: e22152.

[23] Hah YS, Lee WK, Lee S, Kim EJ, Lee JH, Lee SJ, *et al*. β-Sitosterol Attenuates Dexamethasone-Induced Muscle Atrophy via Regulating FoxO1-Dependent Signaling in C2C12 Cell and Mice Model. Nutrients. 2022; 14: 2894.

[24] Hildebrandt L, Dieterlen MT, Klaeske K, Haunschild J, Saeed D, Eifert S, *et al*. Myostatin/AKT/FOXO Signaling Is Altered in Human Non-Ischemic Dilated Cardiomyopathy. Life (Basel, Switzerland). 2022; 12: 1418.

[25] Reed SA, Senf SM, Cornwell EW, Kandarian SC, Judge AR. Inhibition of IkappaB kinase alpha (IKKα) or IKKbeta (IKKβ) plus forkhead box O (Foxo) abolishes skeletal muscle atrophy. Biochemical and Biophysical Research Communications. 2011; 405: 491–496.

[26] Wen Y, Zhang X, Larsson L. Metabolomic Profiling of Respiratory Muscles and Lung in Response to Long-Term Controlled Mechanical Ventilation. Frontiers in Cell and Developmental Biology. 2022; 10: 849973.

[27] Hyatt HW, Ozdemir M, Yoshihara T, Nguyen BL, Deminice R, Powers SK. Calpains play an essential role in mechanical ventilation-induced diaphragmatic weakness and mitochondrial dysfunction. Redox Biology. 2021; 38: 101802.

[28] Shrager JB, Wang Y, Lee M, Nesbit S, Trope W, Konsker H, *et al*. Rationale and design of a mechanistic clinical trial of JAK

inhibition to prevent ventilator-induced diaphragm dysfunction. Respiratory Medicine. 2021; 189: 106620.

[29] Mahmud Z, Tikunova S, Belevych N, Wagg CS, Zhabyeyev P, Liu PB, *et al*. Small Molecule RPI-194 Stabilizes Activated Troponin to Increase the Calcium Sensitivity of Striated Muscle Contraction. Frontiers in Physiology. 2022; 13: 892979.

[30] Rasmussen M, Jin JP. Troponin Variants as Markers of Skeletal Muscle Health and Diseases. Frontiers in Physiology. 2021; 12: 747214.

[31] Hirata Y, Nomura K, Kato D, Tachibana Y, Niikura T, Uchiyama K, *et al*. A Piezo1/KLF15/IL-6 axis mediates immobilization-induced muscle atrophy. The Journal of Clinical Investigation. 2022; 132: 1–13.

[32] Huang Z, Zhong L, Zhu J, Xu H, Ma W, Zhang L, *et al*. Inhibition of IL-6/JAK/STAT3 pathway rescues denervation-induced skeletal muscle atrophy. Annals of Translational Medicine. 2020; 8: 1681.

[33] Dasgupta A, Shukla SK, Vernucci E, King RJ, Abrego J, Mulder SE, *et al*. SIRT1-NOX4 signaling axis regulates cancer cachexia. The Journal of Experimental Medicine. 2020; 217: e20190745.

[34] Powers SK, Ozdemir M, Hyatt H. Redox Control of Proteolysis During Inactivity-Induced Skeletal Muscle Atrophy. Antioxidants & Redox Signaling. 2020; 33: 559–569.

[35] Stana F, Vujovic M, Mayaki D, Leduc-Gaudet JP, Leblanc P, Huck L, *et al*. Differential Regulation of the Autophagy and Proteasome Pathways in Skeletal Muscles in Sepsis. Critical Care Medicine. 2017; 45: e971–e979.

[36] Yang X, Xue P, Chen H, Yuan M, Kang Y, Duscher D, *et al*. Denervation drives skeletal muscle atrophy and induces mitochondrial dysfunction, mitophagy and apoptosis via miR-142a-5p/MFN1 axis. Theranostics. 2020; 10: 1415–1432.

[37] Wang D, Yang Y, Zou X, Zhang J, Zheng Z, Wang Z. Antioxidant Apigenin Relieves Age-Related Muscle Atrophy by Inhibiting Oxidative Stress and Hyperactive Mitophagy and Apoptosis in Skeletal Muscle of Mice. The Journals of Gerontology. Series A, Biological Sciences and Medical Sciences. 2020; 75: 2081–2088.

[38] Yong H, Zhou Y, Ye W, Li T, Wu G, Chen J, *et al*. PINK1/Parkin-mediated mitophagy in mechanical ventilation-induced diaphragmatic dysfunction. Therapeutic Advances in Respiratory Disease. 2021; 15: 1753466621998246.

[39] Moustogiannis A, Philippou A, Zevolis E, Taso OS, Giannopoulos A, Chatzigeorgiou A, *et al*. Effect of Mechanical Loading of Senescent Myoblasts on Their Myogenic Lineage Progression and Survival. Cells. 2022; 11: 3979.

[40] Wang L, Tan Y, Gao L, Lei J, Chen C, Shi Y. Effect of astragaloside on diaphragm cell apoptosis in chronic obstructive pulmonary disease. Food Science & Nutrition. 2020; 8: 6357–6366.

[41] Hanna R, Rozenberg A, Saied L, Ben-Yosef D, Lavy T, Kleifeld O. In-Depth Characterization of Apoptosis N-Terminome Reveals a Link Between Caspase-3 Cleavage and Posttranslational N-Terminal Acetylation. Molecular & Cellular Proteomics: MCP. 2023; 22: 100584.

[42] Changizi Z, Moslehi A, Rohani AH, Eidi A. Chlorogenic acid induces 4T1 breast cancer tumor's apoptosis via p53, Bax, Bcl-2, and caspase-3 signaling pathways in BALB/c mice. Journal of Biochemical and Molecular Toxicology. 2021; 35: e22642.

[43] Khatri M, Naughton RJ, Clifford T, Harper LD, Corr L. The effects of collagen peptide supplementation on body composition, collagen synthesis, and recovery from joint injury and exercise: a systematic review. Amino Acids. 2021; 53: 1493–1506.

[44] Church DD, Hirsch KR, Park S, Kim IY, Gwin JA, Pasiakos SM, *et al*. Essential Amino Acids and Protein Synthesis: Insights into Maximizing the Muscle and Whole-Body Response to Feeding. Nutrients. 2020; 12: 3717.

[45] Harvanova D, Matejova J, Slovinska L, Lacko M, Gulova S, Fecskeova LK, *et al*. The Role of Synovial Membrane in the Development of a Potential In Vitro Model of Osteoarthritis. International Journal of Molecular Sciences. 2022; 23: 2475.

[46] Brzeszczyńska J, Meyer A, McGregor R, Schilb A, Degen S, Tadini V, *et al*. Alterations in the *in vitro* and *in vivo* regulation of muscle regeneration in healthy ageing and the influence of sarcopenia. Journal of Cachexia, Sarcopenia and Muscle. 2018; 9: 93–105.

[47] Giovarelli M, Arnaboldi F, Zecchini S, Cornaghi LB, Nava A, Sommariva M, *et al*. Characterisation of Progressive Skeletal Muscle Fibrosis in the Mdx Mouse Model of Duchenne Muscular Dystrophy: An *In Vivo* and *In Vitro* Study. International Journal of Molecular Sciences. 2022; 23: 8735.

[48] Oxfeldt M, Dalgaard LB, Jørgensen EB, Johansen FT, Dalgaard EB, Ørtenblad N, *et al*. Molecular markers of skeletal muscle hypertrophy following 10 wk of resistance training in oral contraceptive users and nonusers. Journal of Applied Physiology (Bethesda, Md.: 1985). 2020; 129: 1355–1364.

[49] Diao YP, Wu ZY, Chen ZG, Gui L, Miao YQ, Lan Y, *et al*. Mechanism of nerve growth factor promotes angiogenesis and skeletal muscle fiber remodeling in a mouse hindlimb ischemic model. Zhonghua Yi Xue Za Zhi. 2022; 102: 3469–3475.

[50] Powers SK, Demirel HA, Coombes JS, Fletcher L, Calliaud C, Vrabas I, *et al*. Myosin phenotype and bioenergetic characteristics of rat respiratory muscles. Medicine and Science in Sports and Exercise. 1997; 29: 1573–1579.